Progress In Electromagnetics Research M, Vol. 77, 135–145, 2019

A Circularly Polarized Dual-Axis Wide-Angle Rectenna Employing a Dual-Feed Array Antenna with Inclined Patches

Thet Paing Phyoe*, Eisuke Nishiyama, and Ichihiko Toyoda

Abstract—In this paper, a novel circularly polarized rectenna using a dual-feed array antenna with inclined patches is proposed to provide a dual-axis wide-angle reception capability. A new conical and pencil dual-beam circularly polarized array antenna integrating planar magic-Ts is designed and fabricated to overcome the polarization and main-beam misalignment between the transmitting and receiving antennas. To improve the rectenna's output power, open stub matching networks are used to achieve the matching between the antenna and rectifying diodes. Two types of circularly polarized dual-axis rectennas which respectively allow the parallel and series connections of two diodes are experimentally evaluated and compared to confirm the wide-angle reception capabilities in the x-z and y-z planes.

1. INTRODUCTION

In recent years, wireless power transfer has been rapidly developed and has become an attractive application of the microwave technology [1]. Rectenna is one of the most essential elements in wireless power transfer applications, and the improvement of the output DC power is a very important issue. To overcome the issue, several circuit models have been proposed, and the rectenna performance has been analyzed [2, 3]. A high gain array antenna has been presented to improve the rectenna efficiency, and advantages and disadvantages of RF and DC combiner configurations were discussed [4]. However, RF combiner array rectennas have a narrow beam, and the rectenna performance degrades in the case of beam misalignment. Therefore, wide-angle rectennas using a dual-feed network were proposed to solve this issue in the E-plane [5] and H-plane [6]. However, these structures provide wide-angle reception capability in only one plane. A wide-angle rectenna with a triple-feed network has been introduced to provide wide-angle reception capabilities in both E- and H-planes [7]. A wide-angle rectenna that uses a hybrid power combining technique has been reported [8]. Linearly polarized antennas were used in these rectennas [4–8], and strict antenna alignment between the transmitter and receiver is required to obtain a higher output DC power at the load.

Nowadays, circularly polarized (CP) rectennas are very popular and have been proposed to provide better RF-to-DC conversion [9]. However, the CP rectenna in [9] cannot provide constant output DC voltage due to main-beam misalignment. Therefore, the precise main-beam alignment between the transmitter and receiver is required to provide efficient power transfer and constant output DC power. A circularly polarized 2×2 retrodirective Van Atta array rectenna has been presented to track incoming power source signals automatically [10].

In this paper, two CP dual-axis wide-angle rectennas using a new CP dual-feed array antenna with inclined patches are proposed to realize wide-angle reception capabilities in the x-z and y-z planes and overcome the voltage drop due to polarization misalignment. The proposed CP dual-feed array antenna in the proposed rectennas uses in-phase and anti-phase components of the received RF waves to provide

Received 5 October 2018, Accepted 7 December 2018, Scheduled 2 January 2019
* Corresponding author: Thet Paing Phyoe (thet@ceng.ec.saga-u.ac.jp).
The authors are with the Saga University, 1 Honjo-machi, Saga-shi, Saga 840-8502, Japan.

dual-beams such as conical and pencil-beam radiation patterns in the x-z and y-z planes. Two matching open stubs are attached between the antenna and the rectifying diodes to obtain higher output DC power and conversion efficiency. The proposed array antenna is experimentally evaluated to confirm the performance of the antenna such as two different CP radiation patterns, reflection coefficient, isolation and axial ratio. The designed antenna is then evaluated for the wide-angle rectenna by integrating the rectifying circuit, and the output DC voltage of the rectenna is measured with respect to the reception angle, load resistance and RF power density.

2. RECTENNA STRUCTURE

Figure 1 shows the structure of the proposed CP dual-axis wide-angle rectenna using a conical/pencil dual-beam array antenna. Linearly polarized dual-axis conical/pencil dual-beam array antennas using planar magic-Ts have already been presented in [11, 12]. The proposed rectenna consists of four CP microstrip antennas, two magic-Ts, two rectifying diodes, two capacitors, two quarter-wavelength shorted stubs and two matching open stubs. The four CP antenna elements are sequentially rotated as shown in the Figure 1. Antenna elements #1 and #2 are connected to Magic-T1 and #3 and #4 connected to Magic-T2. The slot lines of the magic-Ts are combined and connected to diode D1 via a slot-microstrip line T-junction. On the other hand, the microstrip lines of magic-Ts are combined and connected to diode D2. Quarter-wavelength shorted stubs are attached to the rectifying diodes, and the matching open stubs are attached between the antenna and quarter-wavelength shorted stubs. The microstrip CP antennas and microstrip lines are located on the top side of the substrate, and the slot line and slits are located on the bottom side of the substrate. The rectifying diodes are mounted on the top side of the substrate, and capacitors are placed on the bottom side across the slit of the ground plane. The output voltages of diodes D1 and D2 can be obtained between terminals T1-T2 and T2-T3, respectively. In this configuration, two prototype rectennas are required to confirm wide-angle reception capabilities for the parallel and series connections of the two diodes.

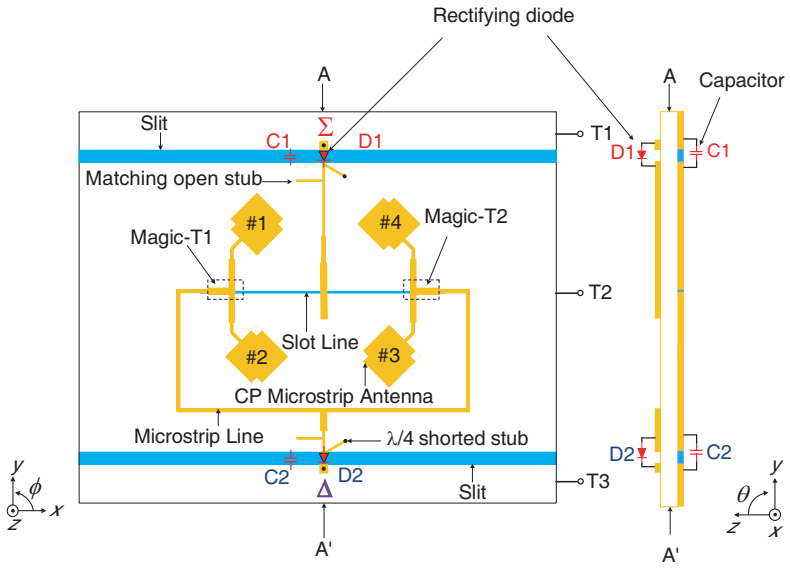

Figure 1. Structure of the proposed circularly polarized dual-axis wide-angle rectenna.

Figure 2 shows the basic concept of the wide-angle rectenna. Two antennas are connected to a magic-T, and RF waves travelling from the direction of the angle θ are received by the two antennas. As the magic-T provides in-phase and anti-phase components of the signals, the sum (Σ) and difference (Δ) of the signals received by the two antenna elements can be expressed as in the following equations:

$$\Sigma = D(\theta)\, e^{j\frac{\varphi}{2}} + D(\theta)\, e^{-j\frac{\varphi}{2}} = 2D(\theta)\cos\frac{\varphi}{2} \tag{1}$$

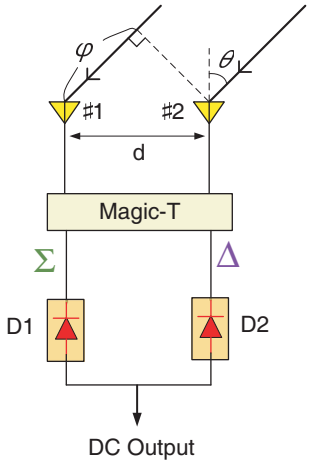

Figure 2. Basic concept of the proposed wide-angle rectenna.

$$\Delta = D(\theta)\,\mathrm{e}^{\mathrm{j}\frac{\varphi}{2}} - D(\theta)\,\mathrm{e}^{-\mathrm{j}\frac{\varphi}{2}} = 2jD(\theta)\sin\frac{\varphi}{2} \tag{2}$$

$$\varphi = \frac{2\pi d}{\lambda}\sin\theta \tag{3}$$

where $D(\theta), \varphi, d$ and λ are the directivity of a single antenna, phase difference of incoming waves, antenna separation, and free-space wavelength, respectively. If the arrival angle θ of the incident waves increases, the phase difference φ of the incident waves also increases, and Σ decreases. The conventional array antennas have a narrow beam, and the antenna's gain rapidly degrades as the arrival angle θ of the incoming waves increases because only Σ is used in the feed networks, and Δ is wasted. However, the performance degradation caused by the phase difference φ of the incoming waves can be recovered using the power of Δ [13].

In the proposed configuration, the in-phase and anti-phase components of the signals are separately rectified by diodes D1 and D2 by effectively using magic-Ts. Then, a wide-angle reception capability is realized by combining the rectified DC voltages of D1 and D2 in series and parallel. In the proposed rectenna, a planar magic-T constructed with a microstrip-line T-junction and slot-microstrip line T-junction is used [14, 15].

3. RECTENNA DESIGN AND PERFORMANCE

This section provides the design and performance of the proposed rectenna. The simulation of the rectifying circuit and antenna design are done in Keysight Technologies' Advanced Design System (ADS) and ADS Momentum.

3.1. Antenna Design and Performance

The design and performance of the proposed dual-feed array antenna are discussed in this section. In this design, a circularly polarized array antenna is used to solve polarization alignment issue and improve antenna gain. The in-phase and anti-phase components of received RF waves are used to provide two different radiation patterns, i.e., pencil- and conical-beams in x-z and y-z planes.

Firstly, a truncated-corner square patch single antenna which provides right-handed circularly polarized (RHCP) radiation is designed at 5.8 GHz. Then, a dual-feed network is designed to provide dual-beam radiation patterns using planar magic-Ts. This antenna can be used as a left-handed circularly polarized (LHCP) antenna by changing the position of the perturbation.

Figures 3 and 4 show phase relations of the antenna elements and simulated 3D radiation patterns of the array antenna. The solid lines on the antenna elements in Figure 3 mean the resultant phase direction of the antenna, and the broken lines stand for x and y axes. When the signal from Port 1

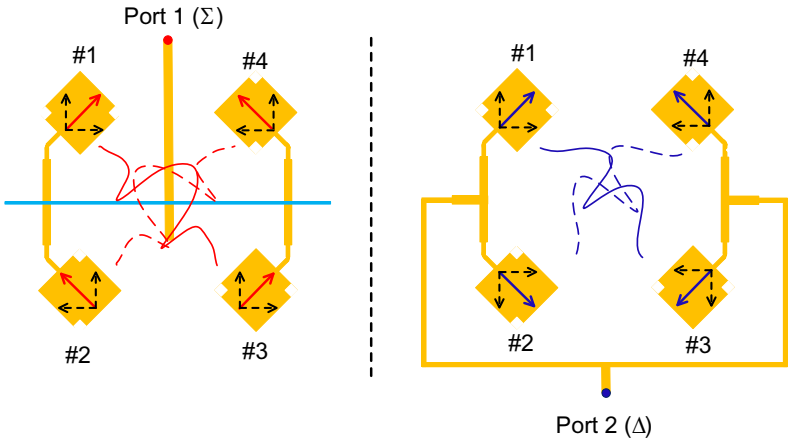

(a) Port 1 feed (b) Port 2 feed

Figure 3. Phase relations of the antenna elements.

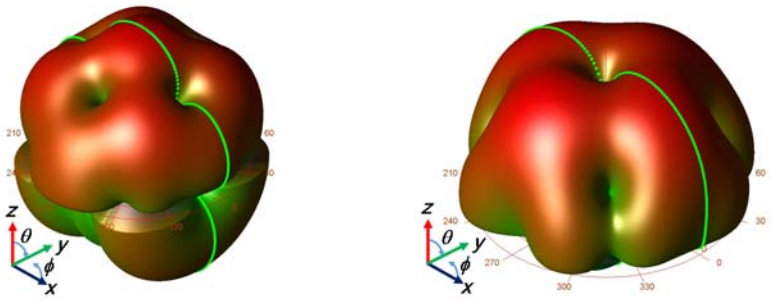

(a) Pencil-beam (Port 1) (b) Conical-beam (Port 2)

Figure 4. Simulated 3D radiation patterns of the proposed array antenna at 5.8-GHz.

excites the antenna elements, the phases of antenna elements #1 and #3 become in-phase, and they make a pencil-beam radiation pattern shown by the solid line in the $-45°$ plane. As shown in Figure 3(a), phases of antenna elements #2 and #4 become in-phase, and they make a pencil-beam radiation pattern shown by the broken lines in the $+45°$ plane. As a result of the combination of these radiation patterns, a pencil-beam radiation pattern shown in Figure 4(a) is obtained.

In Figure 3(b), the phases of antenna elements #1 and #3 become anti-phase when the signal is fed from Port 2, and a conical-beam radiation pattern shown by the solid line is obtained in the $-45°$ plane. Similarly, a conical-beam radiation pattern shown by the broken lines is obtained in the $+45°$ planes when the phases of antenna elements #2 and #4 become anti-phase. As a result, conical-beam radiation pattern shown in Figure 4(b) is obtained by the combination of these radiation patterns. Therefore, pencil- and conical-beam radiation patterns are separately obtained for Port 1 and Port 2, respectively.

Figure 5 shows a prototype of the proposed dual-feed RHCP array antenna designed for 5.8 GHz. In the antenna design, $0.95\lambda_0$ antenna separation which corresponds to the center-to-center of each patch is used to obtain high gain. The substrate is a Teflon glass fiber substrate with a thickness of 0.8 mm, relative dielectric constant of 2.15, and loss tangent of 0.001. The port impedance of the antenna is 50-Ω, and the size of the antenna is 140 mm × 120 mm.

Figure 6 shows the measured and simulated reflection and isolation characteristics of the proposed circularly polarized dual-beam array antenna. The measured 10-dB bandwidth of the reflection coefficient is found around 5.8 GHz. It corresponds to 3.36% with respect to the operating frequency of 5.8 GHz. The isolation between two ports is better than 27 dB.

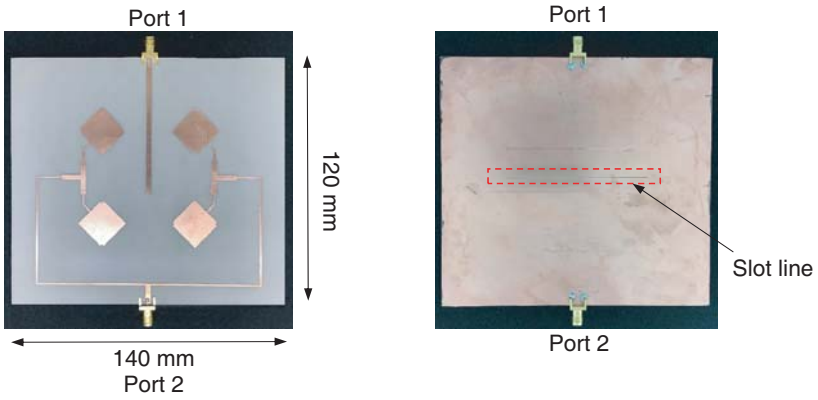

(a) Top view (b) Bottom view

Figure 5. Prototype of the proposed 5.8-GHz circularly polarized array antenna.

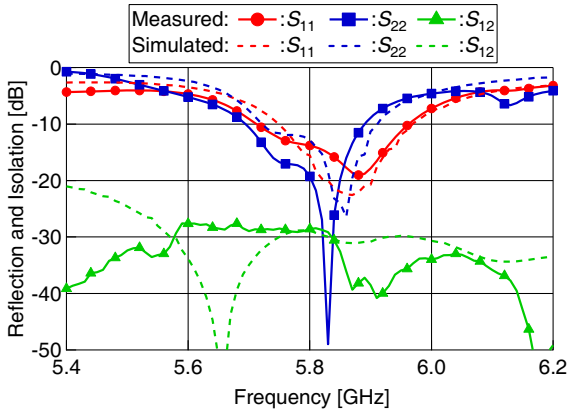

Figure 6. Reflection and isolation characteristics of the proposed antenna.

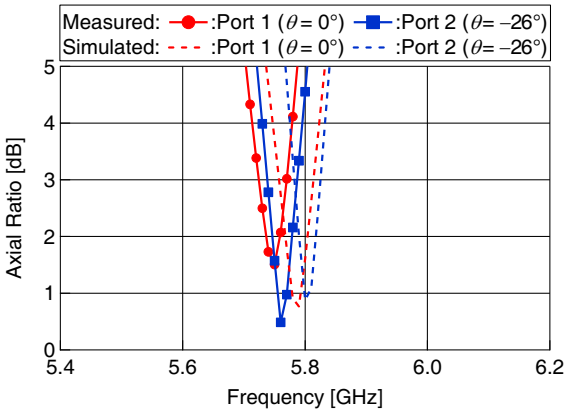

Figure 7. Axial ratio of the proposed antenna.

Figure 7 shows the measured and simulated axial ratio (AR) performances of the antenna. Although the antenna is designed at 5.8 GHz, the measured axial ratio is optimum at 5.75 GHz with the arrival angle of $\theta = 0°$ and $\theta = -26°$, where peak gain is observed for Port 1 and Port 2, respectively. A mismatch between the simulated and measured performances of the antenna is observed because of the slot line imperfection during the fabrication. On the other hand, the difference of the ground plane size can be one of the other reasons for this mismatch because simulation is done with infinite ground plane, and experiment is done with a finite ground plane. A 3-dB axial ratio bandwidth of the antenna is 0.75% with a minimum AR value of 1.5 dB at 5.75 GHz for Port 1 and 0.5 dB at 5.76 GHz for Port 2.

Figure 8 shows the measured and simulated CP radiation patterns of the proposed array antenna at Port 1. The antenna is placed 3 m away from the standard horn antenna in an anechoic chamber to measure far-field radiation patterns. When the signal is fed from Port 1, pencil-beam radiation patterns are obtained in x-z and y-z planes. The solid lines in these figures indicate measured radiation patterns of the antenna at 5.75 GHz where the best AR is obtained, and the broken lines stand for the simulated radiation patterns of the antenna at 5.8 GHz. The cross-polarization level of better than 17 dB is obtained in both planes for RHCP operation. The maximum gain fed from Port 1 is 7.2 dBic at the angle of 0°.

Figure 9 shows the measured and simulated CP radiation patterns of the antenna at Port 2. When the signal is fed from Port 2, conical-beam radiation patterns are obtained in both planes. The cross polarization level of the antenna is better than 17 dB, and the peak gains of the conical-beam radiation pattern are 7 dBic at the angle of −26°.

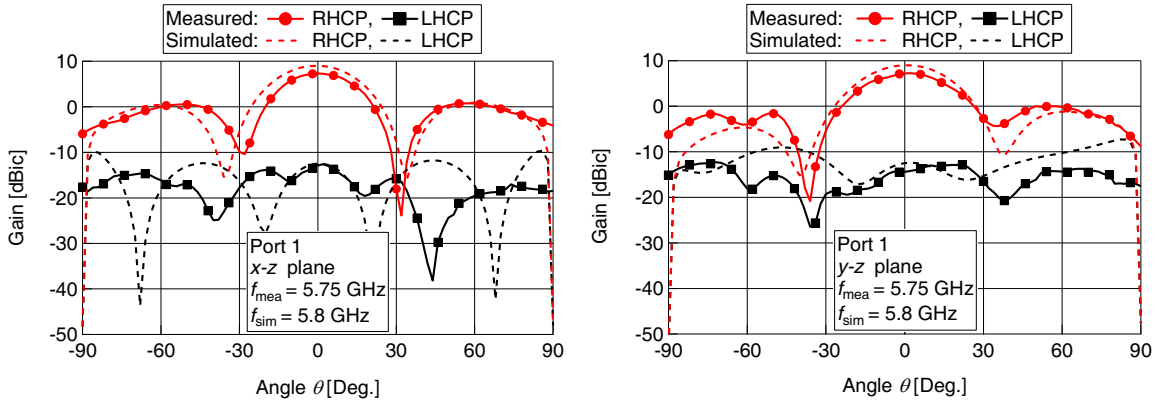

(a) x-z plane (b) y-z plane

Figure 8. CP radiation patterns of the antenna (Port 1).

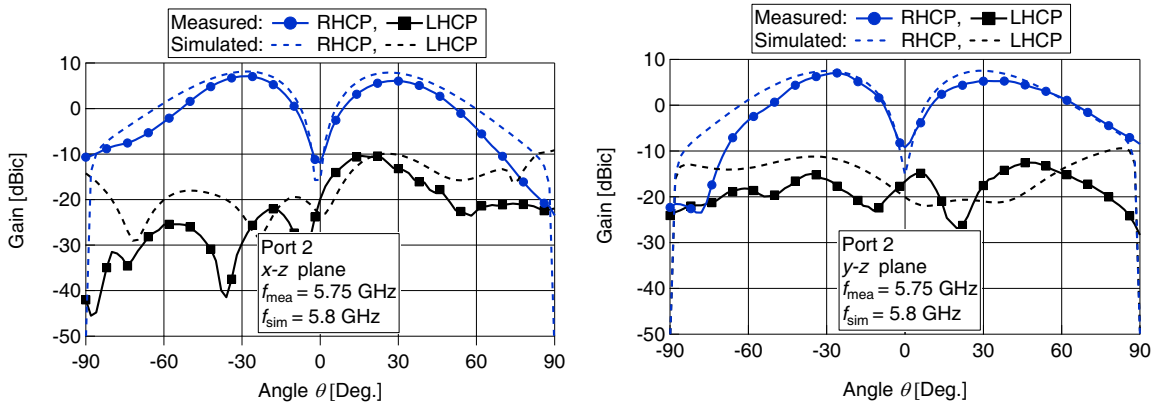

(a) x-z plane (b) y-z plane

Figure 9. CP radiation patterns of the antenna (Port 2).

3.2. Design of Rectifying Circuit

Figure 10 shows an equivalent circuit of the proposed rectenna. Rectenna design using electromagnetic field simulation including nonlinear devices was reported in [16]. However, rectifying circuits and array antenna are separately designed for simplicity in this paper. The RF source corresponds to the antenna, and it is defined by antenna impedance Z_a and received RF power P_{rec}. In this circuit, the matching network is attached to achieve the matching between the antennas and rectifying diode. Experimental

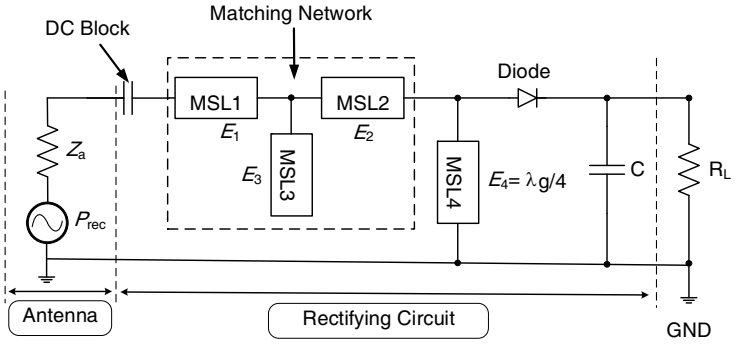

Figure 10. Equivalent circuit of the proposed rectenna.

evaluations of the differential rectennas integrating the matching network have been proposed [17, 18], and advantages and characteristics of the matching networks were discussed in [19].

The matching network in this structure is constructed with three microstrip lines (MSLs), MSL1–MSL3. MSL1 is a feeder line of the antenna, and the maximum output DC power does not depend on its length E_1 when the characteristic impedance of the MSL1 is equal to Z_a. In this design, E_2 and E_3 mean the electrical lengths of the stub position and matching open stub, respectively. The quarter-wavelength shorted stub MSL4 in this figure forms a circuit for charging the direct current to the capacitor and serves to suppress the even harmonic generated by the diode. The characteristic impedance of all microstrip lines in the circuit is 100 Ω, and the matching network is designed at that impedance. In the given condition of 0.04-W/m^2 RF power density and 5.8 GHz, the optimum electrical lengths (E_2 and E_3) of the matching network for the peak gain of the antenna are 59° and 108°, respectively.

Capacitor C makes a short-circuit between separated ground planes and passes DC power to the load. Schottky diodes (MSS20145-B10D, Metelics) are used, and its breakdown voltage is around 0.8 V. The diode acts as a half wave rectifier, and the output DC voltage of the rectenna is measured across the load resistor R_L. The rectenna's conversion efficiency is referred to the percentage of the power converted from RF to DC, and it can be defined as follows:

$$\eta = \frac{P_{DC}}{P_{rec}} \times 100 = \frac{P_{DC}}{P_{PD} \times G_{rec} \times \frac{\lambda^2}{4\pi}} \times 100 \tag{4}$$

where P_{DC}, P_{rec}, P_{PD} and G_{rec} are the output DC power at the load resistance R_L, received RF power, RF power density, and received antenna's gain, respectively. At −13-dBm input RF power and 1-kΩ load resistance, the simulated conversion efficiency of the rectenna without matching network is less than 10%. However, the proposed rectenna with matching network provides higher output DC power, and the conversion efficiency of the rectenna is 54% at the same input RF power and load resistance [19]. Therefore, the conversion efficiency of the proposed CP rectenna integrated with the open stub matching network is higher than those of rectennas in [5–7] because these rectennas have no additional matching network to achieve the matching.

3.3. Performance Analysis on Rectenna

Figure 11(a) is an equivalent circuit of the parallel connection of DC output voltage. In order to combine the two DC outputs in parallel, terminals T1 and T3 are short-circuited, and a load is connected as shown in this figure. In this configuration, the anode terminals of diodes D1 and D2 are connected to the antenna, and the cathode terminal is connected to the terminals.

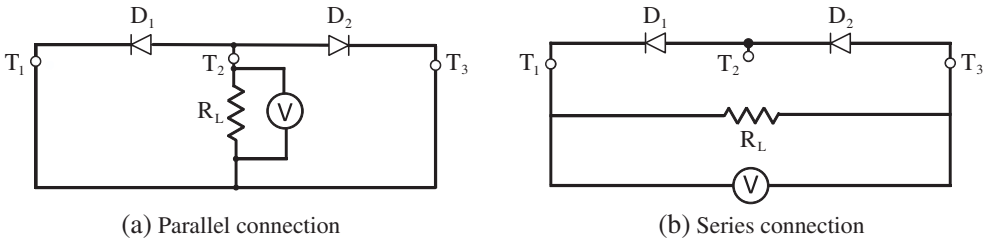

Figure 11. Equivalent circuits.

Figure 11(b) shows an equivalent circuit of a rectenna for series connection. Only the direction of diode D2 is different from the parallel type rectenna as shown in the figure. The DC output power rectified by the two diodes is taken as a series connection between terminals T1 and T3.

Figure 12 shows photographs of the 5.8-GHz band prototype rectenna, and its equivalent circuit is shown in Figure 10. Properties of the substrate are the same as antenna prototype, and the size of the rectenna is 140 mm × 150 mm. Two prototype rectennas are designed and fabricated to connect the two rectifying diodes in series and parallel.

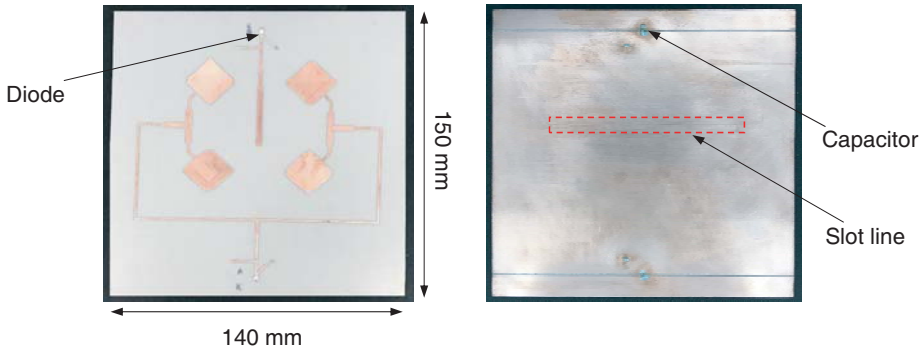

(a) Top plane (b) Bottom plane

Figure 12. Prototype of the proposed 5.8-GHz CP dual-axis wide-angle rectenna.

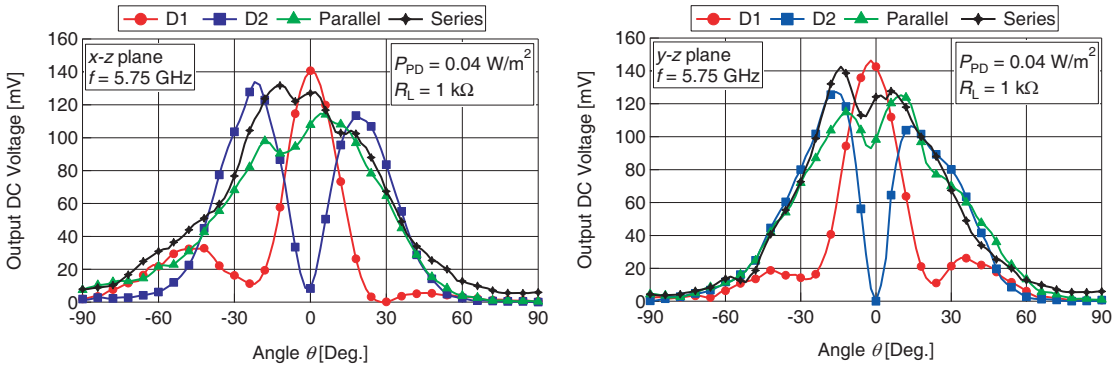

(a) x-z plane (b) y-z plane

Figure 13. Measured output DC voltage vs. angle.

Based on the fabricated CP array antenna and rectenna, a wireless power transfer system is configured in the chamber to measure wide-angle reception capabilities. The fabricated right-handed CP array antenna is used as a transmitting antenna. The rectenna is placed 0.8 m from the transmitting antenna, and the output DC voltages of each rectenna are measured.

Figure 13 shows the measured output DC voltage of the proposed rectenna with respect to the reception angle θ in x-z and y-z planes. They illustrate the performance of the rectenna optimized for the load resistance of 1-kΩ. The measured frequency in this experiment is 5.75 GHz where the best AR is obtained, and the received RF power density is 0.04-W/m^2. When measuring only the in-phase component with D1, terminal T3 is opened. Also, when only the anti-phase component is measured with D2, the measurement is carried out similarly by opening terminal T1.

The measured output DC voltage of the rectenna in the x-z plane is shown in Figure 13(a). In this experiment, the output voltage of diode D1 reaches the maximum value of 140.7 mV when the arrival angle of the radio wave is 0°. However, the output voltage of diode D2 is 133.9 mV when the arrival angle of the radio wave is −22° and 113.4 mV when it is +18°. If diodes D1 and D2 are connected in series, the maximum output voltage is 131.8 mV at the arrival angle of −12°. However, the maximum output voltage of the parallel connection of two diodes is 114.6 mV at the arrival angle of +4°. As shown in Figure 13(b), the maximum output voltages rectified by the diodes are almost the same in the y-z plane. At 0.04-W/m^2 RF power density, better than 70-mV output DC voltages are obtained in the wide reception angle from −30° to +30° in both planes. Therefore, RF power of arriving waves can be effectively converted to DC by separately rectifying in-phase and anti-phase components of the received RF waves.

Figure 14 shows the measured output DC voltage and power with respect to the load resistance. Here, the frequency is 5.75 GHz, and the received RF power density is 0.04-W/m^2. The output voltage

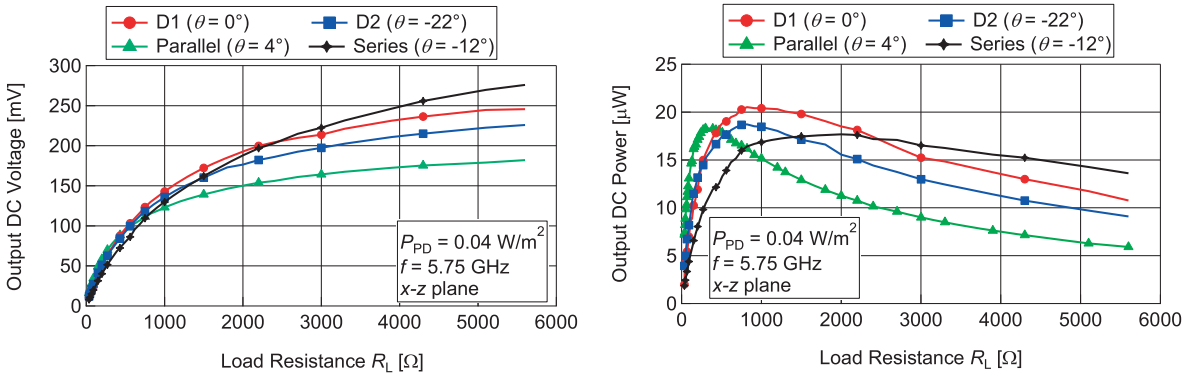

(a) Output DC voltage (b) Output DC power

Figure 14. Measured output DC voltage and power with respect to the load resistance.

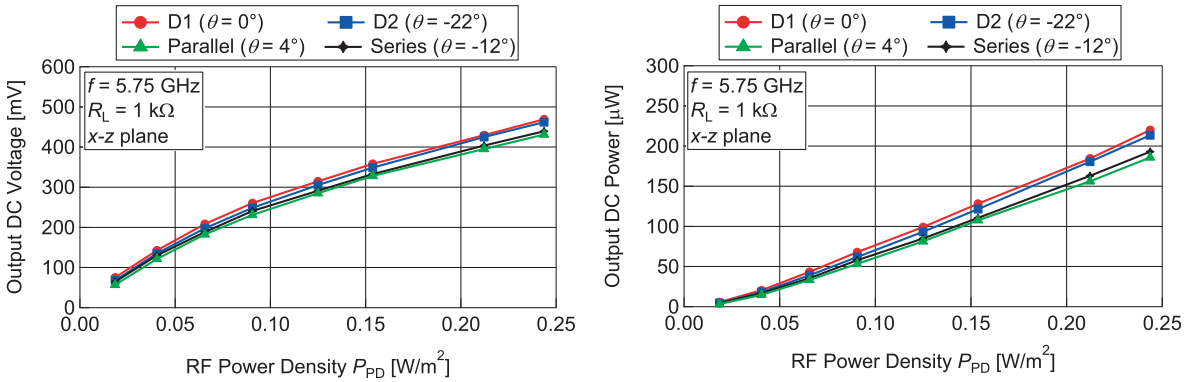

(a) Output DC voltage (b) Output DC power

Figure 15. Measured output DC voltage and power with respect to the RF power density.

of diodes D1, D2, series and parallel connections of two diodes are separately measured. As shown in Figure 14(a), the output DC voltage of the rectenna increases with load resistance. The DC output power in Figure 14(b) is obtained by dividing the square of the measured output voltage by the load resistance, and the load resistance value at which the output power becomes the maximum is taken as the optimum load resistance. The optimum load resistance of diodes D1 and D2 is 820 Ω with the arrival angle of $\theta = 0°$ and $-22°$. Based on Figure 14(b), the conversion efficiency of the rectenna is calculated, and the measured conversion efficiencies of the rectenna at the optimum load resistance are 45% for diode D1 and 41% for diode D2, respectively. However, the optimum load resistance of the series connection of diodes is 1800 Ω with the arrival angle of $-12°$ because the equivalent internal resistances of the two rectifying circuits are connected in series. On the other hand, the optimum load resistance of the parallel connection of diodes is 390 Ω with the arrival angle of 4°.

Figure 15 shows the measured output DC voltage and power with respect to the RF power density. In this experiment, load resistance of 1-kΩ and 5.75 GHz are used. As shown in these figures, the output DC voltage and power dramatically increase with the power density because the rectenna receives more power, and the received voltage of the rectenna is less than the breakdown voltage of the diode.

Figure 16 shows the measured conversion efficiency of the proposed rectenna as a function of the incident RF power density. In the measured RF power density range and 5.75 GHz frequency, the conversion efficiency of the rectenna increases with input power density. The conversion efficiency of the rectenna is nearly constant from the 0.15-W/m^2 RF power density. The output voltage of the rectenna at this power density is around 365 mV, and it is close to the half of diode breakdown voltage (400 mV). At the 0.24-W/m^2 RF power density, the optimum RF-to-DC conversion efficiency of the

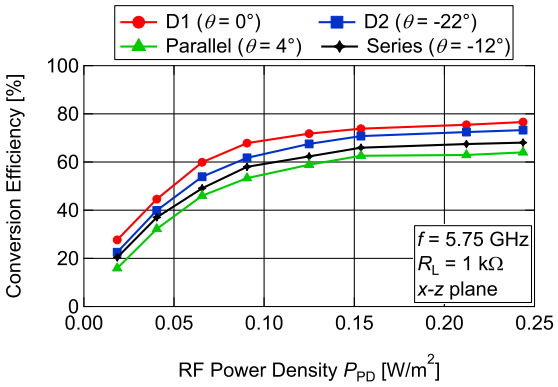

Figure 16. Measured conversion efficiency of the rectenna with respect to RF power density.

Table 1. Comparison of the proposed rectenna with previous rectenna.

Rectennas	Techniques	No. of feeding networks	No. of rectifying circuits	Matching networks	Wide-angle capabilities	Polarization	Structure
[4]	DC combiner	4	4	Yes	x-z plane	Linear	Simple
[5]	RF combiner	2	2	No	y-z plane	Linear	Simple
[7]	RF combiner	3	3	No	x-z and y-z planes	Linear	Simple
[8]	Hybrid (DC & RF) combiner	4	4	Yes	x-z plane	Linear	Not Simple
[10]	Retrodirective Van Atta array	4	2	No	-	Circular	Not Simple
This work	RF combiner	2	2	Yes	x-z and y-z planes	Circular	Simple

rectenna is 75% with 1-kΩ load resistance.

A comparison of the proposed and previous rectennas integrated with four antenna elements is presented in Table 1. As shown in this table, the proposed rectenna has advantages of providing the wide-angle reception capabilities with less feeding networks and rectifying circuits in the x-z and y-z planes. Moreover, the proposed CP rectenna with matching networks generates higher output DC power with a simple structure and reduces the voltage drop due to the polarization alignment in both of the planes.

4. CONCLUSION

In this paper, two novel circularly polarized dual-axis wide-angle rectennas employing a new dual-feed array antenna are examined in detail using two prototype rectennas. A dual-feed CP array antenna is employed to achieve conical and pencil-beam radiation patterns in x-z and y-z planes. It is confirmed that wide-angle reception capabilities are achieved in both of the planes, and higher output DC power is obtained at a low power environment with a simple and compact structure.

ACKNOWLEDGMENT

The authors would like to thank Dr. Takayuki Tanaka, Saga University for his fruitful discussions. This work was supported by JSPS KAKENHI Grant Number 15K06070 and the Cooperative Research Project of Research Institute of Electronics, Shizuoka University.

REFERENCES

1. Brown, W. C., "The history of power transmission by radio wave," *IEEE Trans. Microwave Theory & Tech.*, Vol. 32, No. 9, 1230–1242, 1984.
2. Akkermans, J. A. G., M. C. V. Beurden, G. J. N. Doodeman, and H. J. Visser, "Analytical models for low-power rectenna design," *IEEE Antennas and Wireless Propag. Lett.*, Vol. 4, 187–190, 2005.
3. Shinohara, N., "Rectenna for microwave power transmission," *IEICE Electronics. Express*, Vol. 10, No. 21, 1–13, 2013.
4. Olgun, U., C.-C. Chen, and J. L. Volakis, "Investigation of rectenna array configurations for enhanced RF power harvesting," *IEEE Anten. and Wireless Propag. Lett.*, Vol. 10, 262–265, 2011.
5. Satow, H., E. Nishiyama, and I. Toyoda, "A 5.8-GHz E-plane wide-angle rectenna using magic-Ts," *IEICE Trans. Commun. (Japanese Edition)*, Vol. J99-B, No. 6, 415–423, 2016.
6. Satow, H., Y. Tanaka, E. Nishiyama, and I. Toyoda, "An H-plane wide-angle rectenna using an in-phase/anti-phase dual-feed antenna," *Proc. 2016 Int'l Symp. Antennas and Propag. (ISAP2016)*, POS1-124, 532–533, Okinawa, Japan, 2016.
7. Phyoe, T. P., H. Satow, E. Nishiyama, and I. Toyoda, "A dual-axis wide-angle rectenna using a triple-feed array antenna," *Proc. 2017 Int'l Symp. Antennas and Propag. (ISAP2017)*, 2B4, Phuket, Thailand, 2017.
8. Lee, D.-J., S.-J. Lee, I.-J. Hwang, W.-S. Lee, J.-W. Yu, and K. Chang, "Hybrid power combining rectenna array for wide incident angle coverage in RF energy transfer," *IEEE Trans. Microwave Theory & Tech.*, Vol. 65, No. 9, 3409–3418, 2017.
9. Strassner, B. and K. Chang, "5.8-GHz circularly polarized dual-rhombic-loop traveling-wave rectifying antenna for low power-density wireless power transmission applications," *IEEE Trans. Microwave Theory & Tech.*, Vol. 51, No. 5, 1548–1553, 2003.
10. Ren, Y.-J. and K. Chang, "New 5.8-GHz circularly polarized retrodirective rectenna arrays for wireless power transmission," *IEEE Trans. Microwave Theory & Tech.*, Vol. 54, No. 7, 2970–2976, 2006.
11. Phyoe, T. P., E. Nishiyama, and I. Toyoda, "Design of a conical/pencil dual-beam array antenna using planar magic-Ts," *Proc. 2017 Asian Workshop on Antennas and Propag. (AWAP2017)*, 57–58, Sapporo, Japan, 2017.
12. Phyoe, T. P., E. Nishiyama, and I. Toyoda, "A 5–8-GHz dual-axis monopulse microstrip array antenna using dual-feed network," *Proc. 2018 Asia-Pacific Microwave Conf. (APMC2018)*, FR3-IF-24, Kyoto, Japan, 2018.
13. Toyoda, I. and E. Nishiyama, "Advanced planar rectenna technology," *Proc. 11th Asia-Pacific Eng. Res. Forum on Microwaves and Electromagnetic Theory (APMET2016)*, 1–7, Nagasaki, Japan, 2016.
14. Aikawa, M. and H. Ogawa, "Double-sided MICs and their applications," *IEEE Trans. Microwave Theory & Tech.*, Vol. 37, No. 2, 406–413, 1989.
15. Aikawa, M. and E. Nishiyama, "Compact MIC magic-T and the integration with planar array antenna," *IEICE Trans. Electron.*, Vol. E95-C, No. 10, 1560–1565, 2012.
16. Toyoda, I. and E. Nishiyama, "Rectenna design using electromagnetic field simulation including nonlinear devices," *Proc. 2017 IEEE Int'l Conf. Computational Electromagnetics (ICCEM2017)*, 2B1.5, 130–132, Kumamoto, Japan, 2017.
17. Takahashi, J., E. Nishiyama, and I. Toyoda, "A differential rectenna with matching shorted stubs," *Proc. 2015 IEEE 4th Asia-Pacific Conf. Antennas and Propag. (APCAP2015)*, 445–446, Bail Island, Indonesia, 2015.
18. Takahashi, J., E. Nishiyama, and I. Toyoda, "Experimental study on load resistance design of a differential rectenna," *Proc. 2015 Int'l Symp. Antennas and Propag. (ISAP2015)*, S1.4.1, 223–225, Hobart, Australia, 2015.
19. Phyoe, T. P., H. Satow, E. Nishiyama, and I. Toyoda "Design of a dual-axis wide-angle rectenna with matching networks," *Proc. 2017 Int'l Conf. Science and Engineering (ICSE2017)*, 395–398, Yangon, Myanmar, 2017.